

---

Article

Not peer-reviewed version

---

# MOF-Derived $\text{CoSe}_2$ @ $\text{NiFeOOH}$ Porous Arrays for Efficient Oxygen Evolution Reaction

---

Yulong Tang , Jiangning Li , [Zhiyi Lu](#) , [Yunan Wang](#) \* , [Kai Tao](#) \* , [Yichao Lin](#) \*

Posted Date: 31 August 2023

doi: [10.20944/preprints202308.2177.v1](https://doi.org/10.20944/preprints202308.2177.v1)

Keywords: Oxygen evolution reaction; NiFeOOH; Water electrolysis; Selenidation; CoSe2



Preprints.org is a free multidiscipline platform providing preprint service that is dedicated to making early versions of research outputs permanently available and citable. Preprints posted at Preprints.org appear in Web of Science, Crossref, Google Scholar, Scilit, Europe PMC.

Copyright: This is an open access article distributed under the Creative Commons Attribution License which permits unrestricted use, distribution, and reproduction in any medium, provided the original work is properly cited.

Disclaimer/Publisher's Note: The statements, opinions, and data contained in all publications are solely those of the individual author(s) and contributor(s) and not of MDPI and/or the editor(s). MDPI and/or the editor(s) disclaim responsibility for any injury to people or property resulting from any ideas, methods, instructions, or products referred to in the content.

## Article

# MOF-Derived $\text{CoSe}_2$ @ $\text{NiFeOOH}$ Porous Arrays for Efficient Oxygen Evolution Reaction

Yulong Tang <sup>1,2,†</sup>, Jiangning Li <sup>1,2,†</sup>, Zhiyi Lu <sup>2,3</sup>, Yunan Wang <sup>2,3,\*</sup>, Kai Tao <sup>1,\*</sup> and Yichao Lin <sup>2,3,\*</sup>

<sup>1</sup> School of Materials Science & Chemical Engineering, Ningbo University, Ningbo 315211, China

<sup>2</sup> Ningbo Institute of Materials Technology and Engineering, Chinese Academy of Sciences, Ningbo 315201, China

<sup>3</sup> University of Chinese Academy of Sciences, Beijing 100049, China

\* Correspondence: yclin@nimte.ac.cn (Y.L.); wangyunan@nimte.ac.cn (Y.W.); taokai@nbu.edu.cn (K.T.)

† These authors contributed equally to this work.

**Abstract:** Water electrolysis is a compelling technology for the production of environmentally-friendly hydrogen, minimizing carbon emissions. The electrolysis process of water heavily relies on the effective and steady oxygen evolution reaction (OER) taking place at the anode. Herein, we introduce a highly promising catalyst for OER called  $\text{CoSe}_2$ @ $\text{NiFeOOH}$  arrays, which are supported on a nickel foam. This catalyst, referred to as  $\text{CoSe}_2$ @ $\text{NiFeOOH}/\text{NF}$ , is fabricated through a two-step process involving the selenidation of a Co-based porous metal organic framework and subsequent electrochemical deposition on a nickel foam. The  $\text{CoSe}_2$ @ $\text{NiFeOOH}/\text{NF}$  catalyst demonstrates outstanding activity for the OER in an alkaline electrolyte. It exhibits a low overpotential ( $\eta$ ) of 254 mV at 100 mA cm<sup>-2</sup>, a small Tafel slope of 73 mV dec<sup>-1</sup>, and excellent high stability. The high performance of  $\text{CoSe}_2$ @ $\text{NiFeOOH}/\text{NF}$  can be attributed to the combination of the high conductivity of the inner layer and the synergistic effect between  $\text{CoSe}_2$  and  $\text{NiFeOOH}$ . This study offers an effective method for the fabrication of highly efficient catalysts for the OER.

**Keywords:** Oxygen evolution reaction;  $\text{NiFeOOH}$ ; Water electrolysis; Selenidation;  $\text{CoSe}_2$

## 1. Introduction

The storage of renewable energy presents a significant challenge in constructing an environmentally-friendly energy system.<sup>[1-6]</sup> Water electrolysis has become a promising technology for storing electricity generated from renewable sources by converting it into clean energy carrier,  $\text{H}_2$ . It involves two distinct half-reactions: the hydrogen evolution reaction (HER) occurring at the cathode and the oxygen evolution reaction (OER) taking place at the anode.<sup>[7-10]</sup> Relative to the HER, the OER suffers from a much more sluggish kinetic, which requires highly efficient electrocatalysts. Thus far,  $\text{IrO}_2$  and  $\text{RuO}_2$  represent the state-of-the-art OER electrocatalysts because of their high activity and stability.<sup>[11-16]</sup> However, the high cost and scarcity of these resources limit their extensive utilization.<sup>[12,17-19]</sup> Therefore, it is crucial to develop alternative, affordable electrocatalysts that are abundant in the Earth's crust. Transition-metal chalcogenides (TMCs) with the formula  $\text{M}_x\text{C}_y$  ( $\text{M} = \text{Fe, Co, Ni}$ ;  $\text{C} = \text{S, Se}$ ) have gained significant interest for high performance in OER catalysis, as well as their low-cost and abundance in the Earth's crust.<sup>[20]</sup> Yang Shao-Horn and colleagues conducted a catalytic analysis of perovskite oxide, where they elucidated a correlation between OER activity and the occupancy of 3d electrons with eg symmetry in transition metal cations on the surface. Their findings revealed that an optimized OER electrocatalyst possesses an eg occupancy of approximate one.<sup>[21]</sup> Liu et al. applied this principle to explain the high OER activity of  $\text{CoSe}_2$  which exhibits  $t_{2g}6e_g1$  electronic configuration, approaching the optimal eg filling.<sup>[22,23]</sup> However, they overlooked the surface reconstruction or oxidation of  $\text{CoSe}_2$  under the OER catalysis. The surface oxidation of  $\text{CoSe}_2$  would theoretically lead to the generation of Co oxides or hydroxides on the  $\text{CoSe}_2$  surface. This indicates that the actual catalytic phase is the Co oxides/hydroxides rather than the  $\text{CoSe}_2$ . Therefore, the inner  $\text{CoSe}_2$  serves as an electron-transfer conductor, and is also probably influence the electronic structure of the surface Co oxides/hydroxides.



Based on the above analysis, we incline to believe that the high OER catalytic performance of  $\text{CoSe}_2$  may results from the synergistic effect of the surface oxides and the inner  $\text{CoSe}_2$ . Since  $\text{NiFeOOH}$  species have been recognized as very efficient OER electrocatalysts both from the theoretical calculations and experimental investigations,<sup>[24,25]</sup> we proposed to fabricate thin  $\text{NiFeOOH}$  onto  $\text{CoSe}_2$  surface, aiming to achieve an optimized OER performance through the synergistic effect of  $\text{NiFeOOH}$  and  $\text{CoSe}_2$ . To increase the accessibility of  $\text{CoSe}_2$ , we prepared it by selenidation of a Co-based metal-organic framework (MOF) array grown on Ni foam.<sup>[23,26]</sup> The deposition of  $\text{NiFeOOH}$  onto  $\text{CoSe}_2$  was achieved through electrochemical deposition. The  $\text{CoSe}_2@\text{NiFeOOH}/\text{NF}$  composite exhibited high performance in alkaline electrolytes for the OER, demonstrating an overpotential of 254 mV at a current density of  $100 \text{ mA cm}^{-2}$  and a Tafel slope of  $73 \text{ mV dec}^{-1}$ . Furthermore, it showed excellent stability with negligible current density decay after 100 hours of operation. The high OER activity can be attributed to the increased exposure of active sites, and the synergistic effect of  $\text{NiFeOOH}$  out layer and  $\text{CoSe}_2$  inner layer.

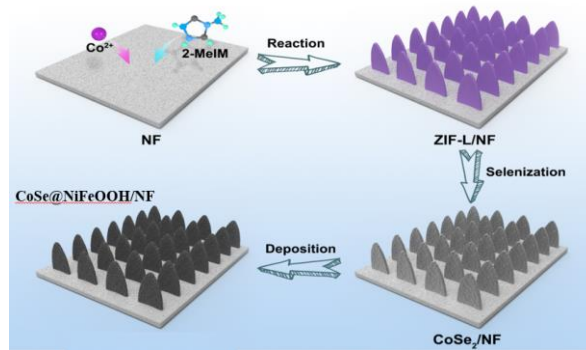


**Figure 1.** Schematic illustration of the routes to  $\text{CoSe}_2@\text{NiFeOOH}/\text{NF}$ .

## 2. Experimental Section

### 2.1. Materials

$\text{Co}(\text{NO}_3)_2 \cdot 6\text{H}_2\text{O}$ , 2-methylimidazole (2-MeIM, 99%),  $\text{Ni}(\text{NO}_3)_2 \cdot 6\text{H}_2\text{O}$ ,  $\text{Fe}(\text{NO}_3)_3 \cdot 9\text{H}_2\text{O}$ , sodium borohydride ( $\text{NaBH}_4$ ), selenium powder (Se) and absolute ethanol were purchased from Aladdin. The Ni Form was obtained from J&K Chemical Technology and subsequently subjected to sonication with acetone, ethanol, and deionized water for 30 minutes each prior to use.

### 2.2. Preparation of cobalt-based ZIF-L/NF

Initially, a solution of  $2 \times 10^{-3}$  mol  $\text{Co}(\text{NO}_3)_2$  and another solution of  $1.6 \times 10^{-2}$  mol 2-MeIM were prepared by dissolving them individually in 40 mL of deionized water in a beaker. Then, the two solutions were combined by stirring. Subsequently, a nickel foam (NF) measuring  $2 \times 3 \text{ cm}$  was immersed in the mixture and left at room temperature for 4 hours to generate ZIF-L/NF. To prepare it for future use, ZIF-L/NF was subjected to three rounds of rinsing with both ethanol and deionized water. Subsequently, it was dried overnight in an oven at  $60^\circ\text{C}$ .

### 2.3. Synthesis of $\text{CoSe}_2/\text{NF}$

The ZIF-L/NF selenidation process was carried out using a hydrothermal method. Initially, 60 mg of  $\text{NaBH}_4$  was completely dissolved in 25 mL of deionized water. Subsequently, 20 mg of selenium powder was added to the solution. The mixture was continuously stirred for 40 minutes until a light-yellow solution was formed. The solution was then transferred into a Teflon-lined stainless-steel autoclave, and a ZIF-L/NF sample with dimensions of  $1 \text{ cm} \times 1.5 \text{ cm}$  was immersed in the solution. The autoclave was kept at a temperature of  $180^\circ\text{C}$  for a duration of 8 hours. Afterward, the resulting  $\text{CoSe}_2/\text{NF}$  product was rinsed with ethanol and water, and finally dried in an oven at a temperature of  $60^\circ\text{C}$  for 12 hours.

#### 2.4. Synthesis of $\text{CoSe}_2@\text{NiFeOOH/NF}$

The  $\text{CoSe}_2@\text{NiFeOOH/NF}$  composite was synthesized by electrochemically deposition with  $\text{CoSe}_2/\text{NF}$  as the working electrode in a solution containing  $\text{Ni}(\text{NO}_3)_2$  and  $\text{Fe}(\text{NO}_3)_3$  (molar ratio of  $\text{Ni}^{2+}/\text{Fe}^{3+} = 4:1$ ). The electrochemical deposition was conducted at a constant potential of -1.4 V vs. RHE for 8 seconds.

#### 2.5. Characterization

X-ray power diffraction (XRD) data were recorded on Bruker D8 ADVANCE DAVINCI. The morphologies and nanostructures were probed by field-emission scanning electron microscopy (SEM, Hitachi S-4800) and transmission electron microscopy (TEM, Tecnai F20, JEM-ARM200F). The surface chemical valences of the samples were analyzed by X-ray photoelectron spectroscopy (XPS) (Axis SUPRA Kratos).

#### 2.6. Electrocatalytic measurement

The electrochemical measurements were conducted on a CHI760E electrochemical workstation. The as-prepared samples served as the working electrode (geometric area:  $1.0 \text{ cm}^2$ ). The counter electrode was a Pt mesh with dimensions of  $1 \text{ cm} \times 1 \text{ cm}$ , and an  $\text{Ag}/\text{AgCl}$  electrode was used as the reference electrode. A 1.0 M KOH electrolyte was utilized. To convert the measured potentials to the reversible hydrogen electrode (RHE) scale, the following equation was used:  $E_{\text{RHE}} = E_{\text{Ag/AgCl}} + 0.059 \text{ pH} + 0.197 \text{ V}$ . Linear sweep voltammetry (LSV) curves were measured at a scan rate of  $5 \text{ mV s}^{-1}$ , while cyclic voltammetry (CV) curves were recorded at scan rates ranging from 10 to  $50 \text{ mV s}^{-1}$ . Electrochemical impedance spectra (EIS) were measured at 1.52 V vs. RHE. All polarization curves were IR-corrected. The double-layer capacitances were determined by analyzing the CV curves obtained at different scan rates, ranging from 10 to  $50 \text{ mV s}^{-1}$ . The stability of the electrocatalyst was evaluated through chrono-amperometry performed at a constant potential. Faraday efficiency (FE) was determined using the bubbling method, following the formula:  $\text{FE} = 4 \times F \times V / (1000 \times V_m \times I_t)$ , where  $V$  is the rising volume (mL) of the soap bubble over time  $t$ ,  $I$  is the current density ( $I_t$  representing the total number of charges transferred under constant current),  $V_m$  is the molar volume ( $24.5 \text{ L mol}^{-1}$  at  $25^\circ\text{C}$ ), and  $F$  is the Faraday constant ( $96485 \text{ C mol}^{-1}$ ).

### 3. Results and Discussion

ZIF-L was deposited onto NF prepared by facilely immersing NF into a solution of cobalt nitrate and 2-methylimidazole at room temperature. The morphology of the ZIF-L/NF sample was analyzed by SEM, which allows for detailed imaging of the sample surface at high magnification. The crystal structure of the synthesized catalyst was determined using powder XRD. Figure 2a, d, and g illustrate the triangular ZIF-L plates with smooth surfaces vertically aligned on the NF. The sharp diffraction peaks at  $44.5^\circ$ ,  $51.9^\circ$ , and  $76.2^\circ$  are attributed to the Ni substrate, and the peak at  $29.4^\circ$  belongs to ZIF-L. This confirms the successful fabrication of ZIF-L on NF. After selenization, ZIF-L transformed into  $\text{CoSe}_2$  phase while maintaining its morphology, except that the surface became rougher (Figure 2b, e, and h). Subsequently,  $\text{NiFeOOH}$  was electrochemically deposited onto  $\text{CoSe}_2$ , resulting in a morphological change where  $\text{CoSe}_2$  formed an array with increased surface roughness and additional folds. XRD analysis of the  $\text{CoSe}_2@\text{NiFeOOH/NF}$  sample showed no visible peaks except those of the Ni substrate, suggesting the amorphous structure in the  $\text{NiFeOOH}$  layer. <sup>[27]</sup> The absence of XRD signals for  $\text{CoSe}_2$  demonstrates that a relatively compact  $\text{NiFeOOH}$  layer is formed on the  $\text{CoSe}_2$  surface. The three-dimensional  $\text{CoSe}_2@\text{NiFeOOH}$  can aid in the transportation of electrolytes and the diffusion of reactive gases, thereby accelerating the reaction process. <sup>[27]</sup>

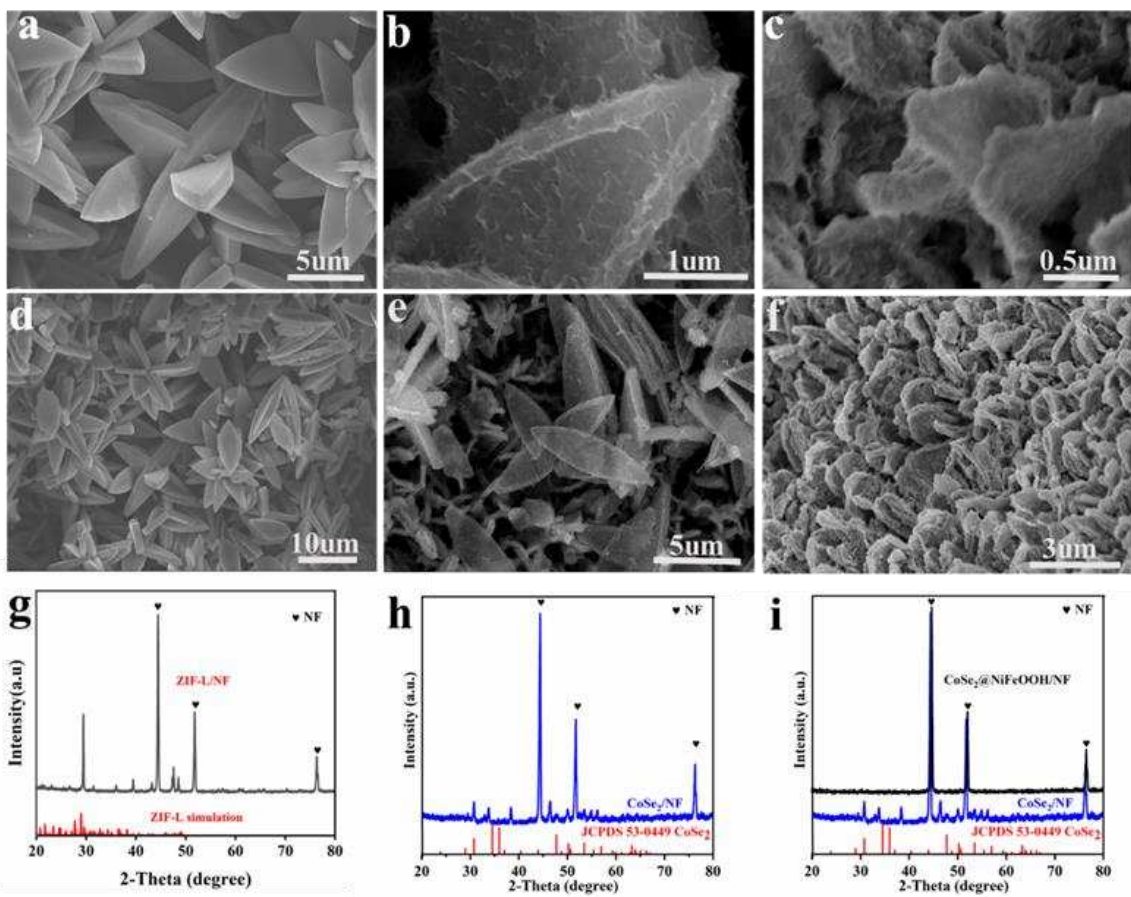


**Figure 2.** SEM images of (a, d) ZIF-L, (b, e) CoSe<sub>2</sub> and (c, f) CoSe<sub>2</sub>@NiFeOOH/NF. XRD pattern of (g) ZIF-L/NF, (h) CoSe<sub>2</sub>/NF, (i) CoSe<sub>2</sub>@NiFeOOH/NF.

The detailed morphology of CoSe<sub>2</sub>@NiFeOOH was further characterized by TEM. Figure 1a shows that CoSe<sub>2</sub>@NiFeOOH possesses a thin-leaf like morphology. The weak polycrystalline rings in the selected area electron diffraction (SAED) pattern (Figure 2c) indicate the poor crystallization of these thin-leaf structures in the single derived CoSe<sub>2</sub>@NiFeOOH. (Figure 2c). The structure of CoSe<sub>2</sub>@NiFeOOH/NF was precisely characterized using high-resolution TEM (HRTEM). At the top surface of CoSe<sub>2</sub>@NiFeOOH, two fringes with lattice spacings of 0.259 and 0.223 nm are observed, corresponding to the (111) and (210) planes of CoSe<sub>2</sub>, respectively. Elemental mapping images demonstrate the homogeneous dispersion of Ni, Fe, Co, Se, and O elements throughout the entire CoSe<sub>2</sub>@NiFeOOH/NF.

X-ray photoelectron spectroscopy (XPS) measurements were performed to analyze the elemental composition and chemical valence states of the as-prepared CoSe<sub>2</sub>@NiFeOOH/NF. As shown in Figure 3a, two peaks centered at 855.7 and 873.5 eV were identified as the main peaks corresponding to oxidized Ni 2p<sub>3/2</sub> and Ni 2p<sub>1/2</sub>, respectively. Another two peaks at 861.2 and 879.3 eV were attributed to the shakeup satellite peak. [28] Figure 3b displays the Co 2p<sub>1/2</sub> and Co 2p<sub>3/2</sub> peaks, which can be further divided into four peaks located at 796.8/780.8 eV (Co<sup>2+</sup>) and 783.8/802.2 eV (Co<sup>3+</sup>). This suggests that the Co atom in CoSe<sub>2</sub>@NiFeOOH/NF is predominantly in the valence states of +2 and +3. [28] In the XPS spectra of Fe 2p (Figure 3c), two characteristic peaks at 712.9 and 726.1 eV correspond to Fe 2p<sub>3/2</sub> and Fe 2p<sub>1/2</sub>, respectively, indicating the presence of Fe<sup>3+</sup>. [29] The findings collectively indicate that Ni and Fe exist as Ni and Fe oxidation states in CoSe<sub>2</sub>@NiFeOOH/NF. Furthermore, the analysis of the Se 3d peak reveals that the peak at 54.5 eV corresponds to Se 3d in CoSe<sub>2</sub>@NiFeOOH/NF, and the presence of a peak at 59.2 eV indicates bonding between Se and O, confirming the surface oxidation of Se species. [30-33]

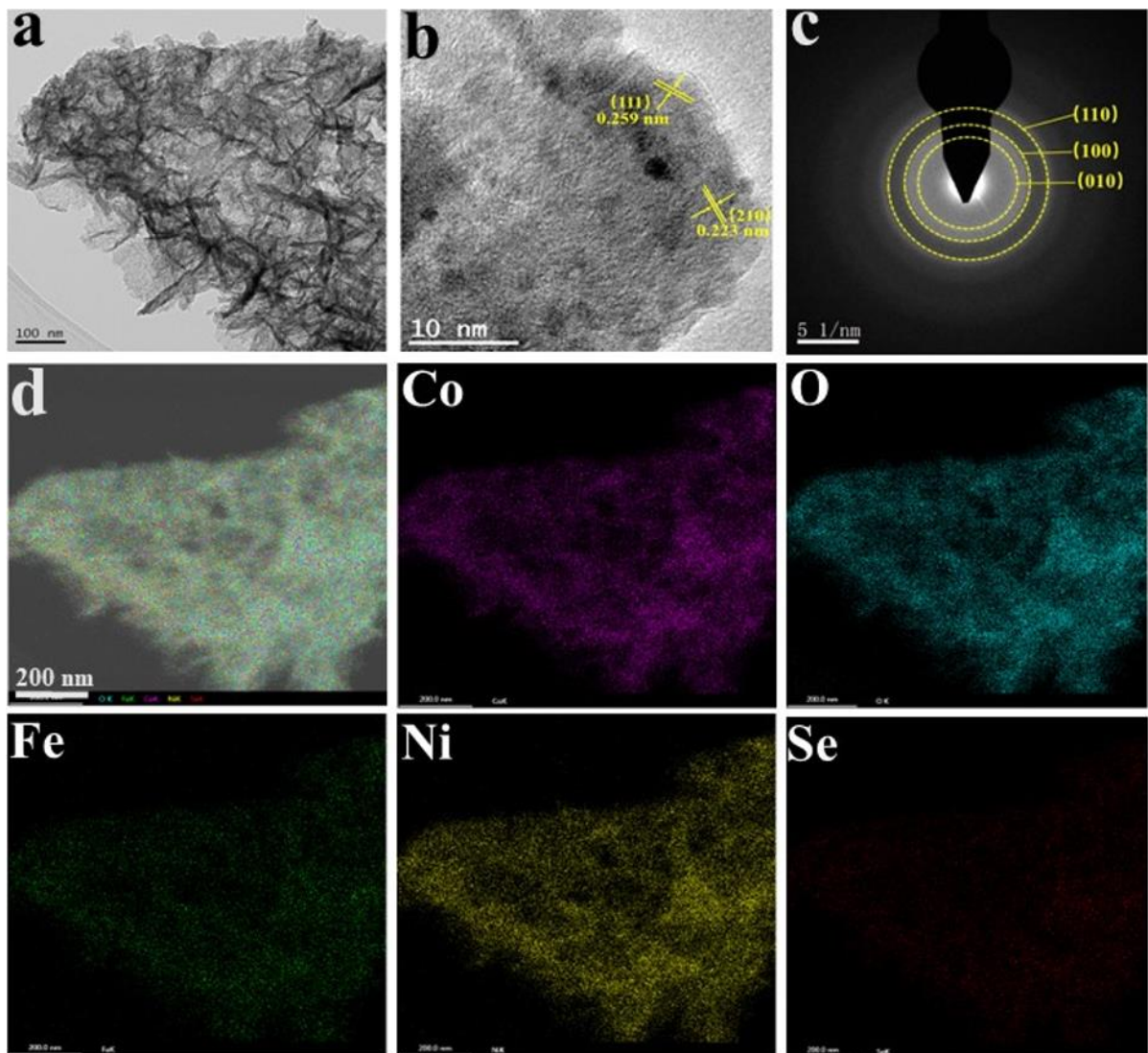


**Figure 3.** (a) TEM, (b) HRTEM, (c) SAED pattern, and (d) STEM images and the corresponding elemental mapping images of Co, O, Fe, Ni and Se of  $\text{CoSe}_2@\text{NiFeOOH}/\text{NF}$ .

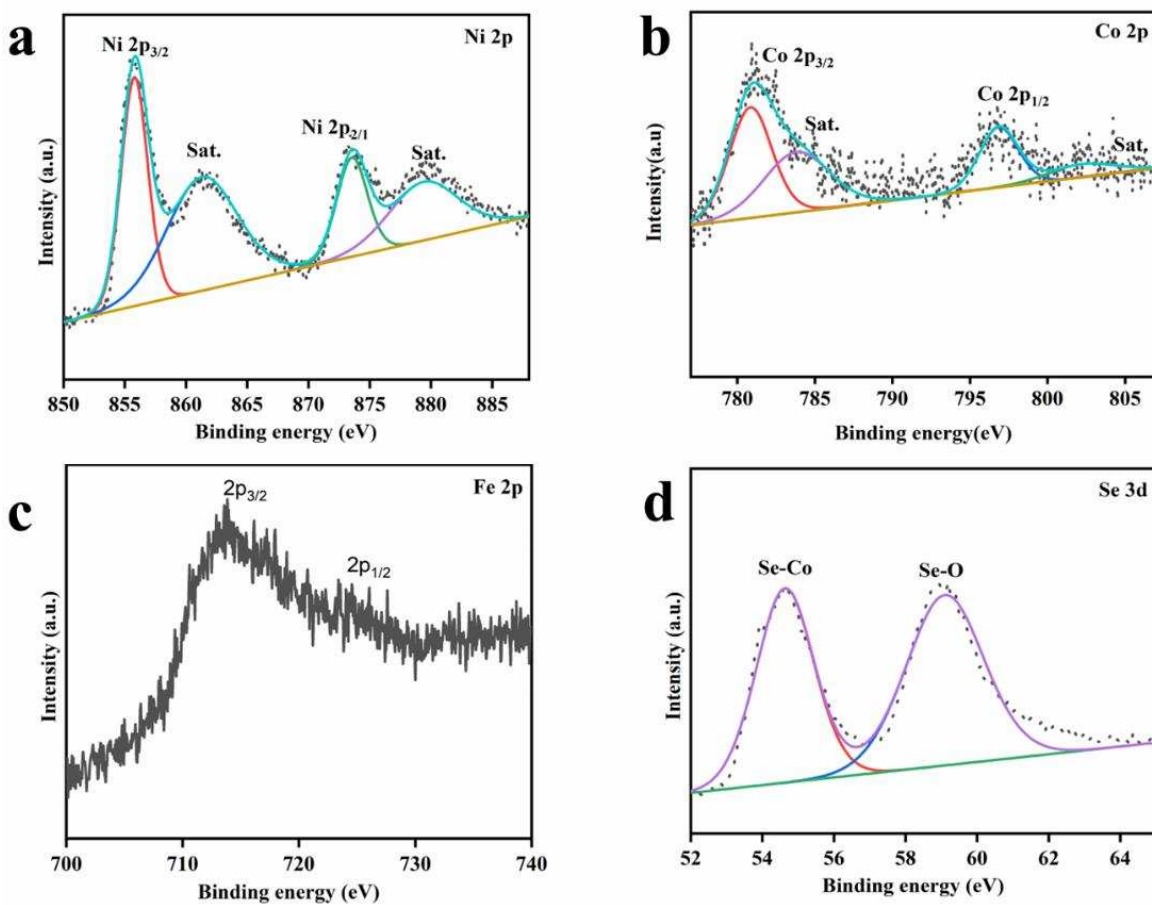


**Figure 4.** High-resolution XPS spectra of CoSe<sub>2</sub>@NiFeOOH/NF.

The catalysts' OER performance was assessed using an electrochemical three-electrode system in a 1 M KOH alkaline solution. As shown in Figure 5a, CoSe<sub>2</sub>@NiFeOOH/NF exhibits an overpotential of 254 mV at 100 mA cm<sup>-2</sup>, which is significantly lower than that of CoSe<sub>2</sub>/NF, NiFe-LDH/NF, NF/Selenization, CoSe<sub>2</sub>@NiOOH/NF, and CoSe<sub>2</sub>@FeOOH/NF. The OER activity of CoSe<sub>2</sub>@NiFeOOH/NF is also among the best OER electrocatalysts reported. (Table S1). The Tafel slopes of the four samples, namely CoSe<sub>2</sub>@FeOOH/NF, CoSe<sub>2</sub>@NiOOH/NF, CoSe<sub>2</sub>/NF, and CoSe<sub>2</sub>@NiFeOOH/NF, were calculated to analyze their kinetics. As shown in Figure 5c, CoSe<sub>2</sub>@NiFeOOH possesses the smallest Tafel slope of 73 mV dec<sup>-1</sup>, much smaller than those of CoSe<sub>2</sub>@FeOOH/NF (102 mV dec<sup>-1</sup>), CoSe<sub>2</sub>/NF (119 mV dec<sup>-1</sup>) and CoSe<sub>2</sub>@NiOOH/NF (126 mV dec<sup>-1</sup>), suggesting a faster OER kinetics. To gain further insight into the kinetics of electron transfer, EIS measurements were performed. Figure 5b displays the Nyquist plots of all the samples. Notably, the CoSe<sub>2</sub>@NiFeOOH/NF sample exhibits the smallest diameter of the semicircle in the high frequency region, which unequivocally confirms the presence of charge-transfer resistance ( $R_{ct}$ ). This resistance facilitates smooth charge transfer, ultimately resulting in excellent oxygen evolution reaction (OER) activity. Additionally, to understand the intrinsic catalytic activity of CoSe<sub>2</sub>@NiFeOOH/NF for OER, the electrochemical surface area (ECSA) was estimated by measuring the double-layer capacitance ( $C_{dl}$ ) in the potential range of 1.07-1.17 V at scan rates ranging from 10 to 50 mV s<sup>-1</sup> (Figure S1). Interestingly, CoSe<sub>2</sub>@NiFeOOH/NF exhibits the highest  $C_{dl}$  value of 29.0 mF cm<sup>-2</sup> among all the samples, surpassing those of CoSe<sub>2</sub>@NiOOH/NF (23.1 mF cm<sup>-2</sup>) and CoSe<sub>2</sub>@FeOOH/NF (20.5 mF cm<sup>-2</sup>). Furthermore, the electrocatalytic stability of CoSe<sub>2</sub>@NiFeOOH/NF was evaluated. As depicted in Figure 5h, the current variation is negligible after a 100-hour continuous test at 1.54 V. The overpotential increase for every 50 mA cm<sup>-2</sup> of current density is illustrated in Figure 5f. It is evident

from the Figure 5a that  $\text{CoSe}_2@\text{NiFeOOH}/\text{NF}$  has a significantly lower overpotential than  $\text{CoSe}_2@\text{FeOOH}/\text{NF}$  and  $\text{CoSe}_2@\text{NiOOH}/\text{NF}$ , signifying higher catalytic activity of  $\text{CoSe}_2@\text{NiFeOOH}$ . Figure 5e illustrates the chrono-potentiometric curve of  $\text{CoSe}_2@\text{NiFeOOH}$ , showing multiple steps with the current density incrementing from 10 to 100  $\text{mA cm}^{-2}$  in ten steps. In the initial step, the potential rapidly stabilizes at 1.44 V and remains nearly constant for a duration of 320 s. Similar phenomena are observed in the subsequent steps, indicating the exceptional mass transport and electronic conductivity characteristics of  $\text{CoSe}_2@\text{NiFeOOH}/\text{NF}$ . The faradaic efficiency for OER on the  $\text{CoSe}_2@\text{NiFeOOH}/\text{NF}$  electrodes was evaluated by measuring the  $\text{O}_2$  produced during a constant current test experiment. According to Figure 4g, the measured amount of  $\text{O}_2$  is in close agreement with the theoretical yield, resulting in a remarkable faradaic efficiency of 97.8% for the  $\text{CoSe}_2@\text{NiFeOOH}/\text{NF}$  electrode.

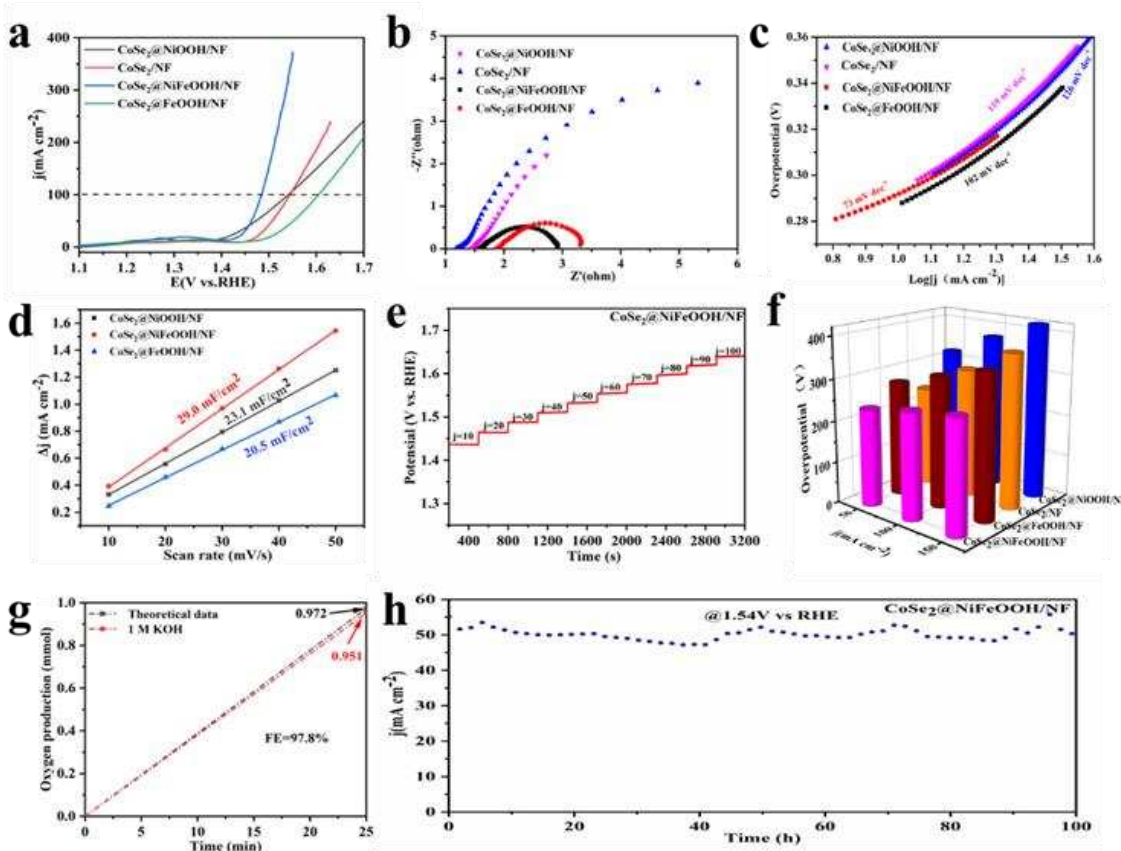


**Figure 5.** (a) LSV curves for  $\text{CoSe}_2/\text{NF}$ ,  $\text{CoSe}_2@\text{FeOOH}/\text{NF}$ ,  $\text{CoSe}_2@\text{NiOOH}/\text{NF}$ ,  $\text{NiFe-LDH}/\text{NF}$ ,  $\text{NF}/\text{Selenization}$  and  $\text{CoSe}_2@\text{NiFeOOH}/\text{NF}$ . (b) EIS curves, (c) Tafel plots, (d)  $C_{dl}$  plots. (e) Rate capability evaluation of  $\text{CoSe}_2@\text{NiFeOOH}/\text{NF}$ . (f) Catalyst overpotentials at different current densities. (g) Faraday efficiency. (h) i-t curve for  $\text{CoSe}_2@\text{NiFeOOH}$  at the  $\eta=0.31$  V for 100 h.

#### 4. Conclusions

In summary, a three-dimensional  $\text{CoSe}_2@\text{NiFeOOH}$  supported on nickel foam for efficient OER catalysis was fabricated. The excellent conductivity of  $\text{CoSe}_2$  and the synergistic effect between  $\text{CoSe}_2$  and  $\text{NiFeOOH}$  facilitate the OER catalysis on  $\text{CoSe}_2@\text{NiFeOOH}/\text{NF}$ . The  $\text{CoSe}_2@\text{NiFeOOH}/\text{NF}$  catalyst demonstrated excellent performance in the alkaline electrolyte achieving an overpotential of 254 mV at 100  $\text{mA cm}^{-2}$  and a Tafel slope of 73 mV dec<sup>-1</sup>. Furthermore, the catalyst demonstrated remarkable stability with minimal decay in current density, even after 100 hours. The findings of this study represent a prototype of a synergistic strategy for creating highly efficient electrocatalysts.

**Supplementary Materials:** The following supporting information can be downloaded at the website of this paper posted on Preprints.org. Figure S1. CV curves of a)  $\text{CoSe}_2@\text{FeOOH}/\text{NF}$ . b)  $\text{CoSe}_2@\text{NiFeOOH}/\text{NF}$  and c)  $\text{CoSe}_2@\text{NiOOH}/\text{NF}$ . Table S1. Comparison of the OER activity of  $\text{CoSe}_2@\text{NiFeOOH}/\text{NF}$  with other non-noble metal electrocatalysts in alkaline solution.

**Author Contributions:** Conceptualization, Y.L., Y.W. and K.T.; methodology, Y.L., Y.T., Z.L. and J.L.; formal analysis, J.L., Y.T., Y.W. and Y.L.; investigation, Y.T. and J.L.; data curation, Y.T. and J.L.; writing—original draft preparation Y.T. and J.L.; writing—review and editing, Y.L. and Y.W.; supervision, Y.L., and K.T.; project administration, Y.L. Y.T. and J.L.; funding acquisition, Y.L. and Y.W. All authors have read and agreed to the published version of the manuscript.

**Funding:** This research was funded by R&D Program of Zhejiang (No. 2022C01029), National Natural Science Foundation of China (No. 52271232), Bellwethers Project of Zhejiang Research and Development Plan (2022C01158), Natural Science Foundation of Zhejiang Province (No. LY21E020008), Youth Innovation Promotion Association, CAS (No. 2020300), Ningbo S&T Innovation 2025 Major Special Program (2022Z205), and Jiangbei Science and Technology planning project (202301A09).

**Data Availability Statement:** We would like to share our data upon request from the authors.

**Conflicts of Interest:** The authors declare no conflict of interest.

## References

1. Dresp, S.; Ngo Thanh, T.; Klingenhof, M.; Brückner, S.; Hauke, P.; Strasser, P. Efficient direct seawater electrolyzers using selective alkaline NiFe-LDH as OER catalyst in asymmetric electrolyte feeds. *Energy Environ. Sci.* **2020**, *13*, 1725-1729.
2. Wang, Y.; Tao, S.; Lin, H.; Wang, G.; Zhao, K.; Cai, R.; Tao, K.; Zhang, C.; Sun, M.; Hu, J.; Huang, B.; Yang, S. Atomically targeting NiFe LDH to create multivacancies for OER catalysis with a small organic anchor. *Nano Energy.* **2021**, *81*, 105606.
3. Sun, H.; Zhang, W.; Li, J.-G.; Li, Z.; Ao, X.; Xue, K.-H.; Ostrikov, K. K.; Tang, J.; Wang, C. Rh-engineered ultrathin NiFe-LDH nanosheets enable highly-efficient overall water splitting and urea electrolysis. *Appl. Catal. B Environ.* **2021**, *284*, 119740.
4. Alabaid, A.; Wang, C.; Adomaitis, R. A. Mechanism and kinetics of HER and OER on NiFe LDH films in an alkaline electrolyte. *J. Electrochem. Soc.* **2018**, *165*, J3395-J3404.
5. Hunter, B. M.; Hieringer, W.; Winkler, J. R.; Gray, H. B.; Müller, A. M. Effect of interlayer anions on NiFe-LDH nanosheet water oxidation activity. *Energy Environ. Sci.* **2016**, *9*, 1734-1743.
6. Wang, Y.; Yan, D.; El Hankari, S.; Zou, Y.; Wang, S. Recent progress on layered double hydroxides and their derivatives for electrocatalytic water splitting. *Adv. Sci.* **2018**, *5*, 1800064.
7. Tang, Y.; Liu, Q.; Dong, L.; Wu, H. B.; Yu, X.-Y. Activating the hydrogen evolution and overall water splitting performance of NiFe LDH by cation doping and plasma reduction. *Appl. Catal. B Environ.* **2020**, *266*, 118627.
8. Hu, L.; Zeng, X.; Wei, X.; Wang, H.; Wu, Y.; Gu, W.; Shi, L.; Zhu, C. Interface engineering for enhancing electrocatalytic oxygen evolution of NiFe LDH/NiTe heterostructures. *Appl. Catal. B Environ.* **2020**, *273*, 119014.
9. Nayak, S.; Parida, K. Superactive NiFe-LDH/graphene nanocomposites as competent catalysts for water splitting reactions. *Inorg. Chem. Front.* **2020**, *7*, 3805-3836.
10. Yu, J.; Yu, F.; Yuen, M.-F.; Wang, C. Two-dimensional layered double hydroxides as a platform for electrocatalytic oxygen evolution. *J. Mater. Chem. A* **2021**, *9*, 9389-9430.
11. Chen, S.; Huang, H.; Jiang, P.; Yang, K.; Diao, J.; Gong, S.; Liu, S.; Huang, M.; Wang, H.; Chen, Q. Mn-doped RuO<sub>2</sub> nanocrystals as highly active electrocatalysts for enhanced oxygen evolution in acidic media. *ACS Catal.* **2019**, *10*, 1152-1160.
12. Hubert, M. A.; Patel, A. M.; Gallo, A.; Liu, Y.; Valle, E.; Ben-Naim, M.; Sanchez, J.; Sokaras, D.; Sinclair, R.; Nørskov, J. K.; King, L. A.; Bajdich, M.; Jaramillo, T. F. Acidic oxygen evolution reaction activity–stability relationships in Ru-based pyrochlores. *ACS Catal.* **2020**, *10*, 12182-12196.
13. Su, J.; Ge, R.; Jiang, K.; Dong, Y.; Hao, F.; Tian, Z.; Chen, G.; Chen, L. Assembling ultrasmall Copper-doped ruthenium oxide nanocrystals into hollow porous polyhedra: highly robust electrocatalysts for oxygen evolution in acidic media. *Adv. Mater.* **2018**, *30*, 1801351.
14. Jin, H.; Choi, S.; Bang, G. J.; Kwon, T.; Kim, H. S.; Lee, S. J.; Hong, Y.; Lee, D. W.; Park, H. S.; Baik, H.; Jung, Y.; Yoo, S. J.; Lee, K. Safeguarding the RuO<sub>2</sub> phase against lattice oxygen oxidation during acidic water electrooxidation. *Energy Environ. Sci.* **2022**, *15*, 1119-1130.
15. Lin, Y.; Tian, Z.; Zhang, L.; Ma, J.; Jiang, Z.; Deibert, B. J.; Ge, R.; Chen, L. Chromium-ruthenium oxide solid solution electrocatalyst for highly efficient oxygen evolution reaction in acidic media. *Nat. Commun.* **2019**, *10*, 162-175.
16. Retuerto, M.; Pascual, L.; Calle-Vallejo, F.; Ferrer, P.; Gianolio, D.; Pereira, A. G.; Garcia, A.; Torrero, J.; Fernandez-Diaz, M. T.; Bencok, P.; Pena, M. A.; Fierro, J. L. G.; Rojas, S. Na-doped ruthenium perovskite electrocatalysts with improved oxygen evolution activity and durability in acidic media. *Nat. Commun.* **2019**, *10*, 2041-2050.

17. An, L.; Wei, C.; Lu, M.; Liu, H.; Chen, Y.; Scherer, G. G.; Fisher, A. C.; Xi, P.; Xu, Z. J.; Yan, C. H. Recent development of oxygen evolution electrocatalysts in acidic environment. *Adv. Mater.* **2021**, *33*, e2006328.
18. Li, L.; Wang, P.; Shao, Q.; Huang, X. Recent progress in advanced electrocatalyst design for acidic oxygen evolution reaction. *Adv. Mater.* **2021**, *33*, e2004243.
19. Spori, C.; Kwan, J. T. H.; Bonakdarpour, A.; Wilkinson, D. P.; Strasser, P. The stability challenges of oxygen evolving catalysts: towards a common fundamental understanding and mitigation of catalyst degradation. *Angew. Chem. Int. Ed.* **2017**, *56*, 5994-6021.
20. Zhang, T.; Hang, L.; Sun, Y.; Men, D.; Li, X.; Wen, L.; Lyu, X.; Li, Y. Hierarchical hetero-Ni3Se4@NiFe LDH micro/nanosheets as efficient bifunctional electrocatalysts with superior stability for overall water splitting. *Nanoscale Horiz.* **2019**, *4*, 1132-1138.
21. Suntivich, J.; May, K. J.; Gasteiger, H. A.; Goodenough, J. B.; Shao-Horn, Y. A perovskite oxide optimized for oxygen evolution catalysis from molecular orbital principles. *Science* **2011**, *334*, 1383-1385.
22. Liu, Y.; Cheng, H.; Lyu, M.; Fan, S.; Liu, Q.; Zhang, W.; Zhi, Y.; Wang, C.; Xiao, C.; Wei, S.; Ye, B.; Xie, Y. Low overpotential in vacancy-rich ultrathin CoSe2 nanosheets for water oxidation. *J. Am. Chem. Soc.* **2014**, *136*, 15670-15675.
23. Li, J. G.; Sun, H.; Lv, L.; Li, Z.; Ao, X.; Xu, C.; Li, Y.; Wang, C. Metal-organic framework-derived hierarchical (Co,Ni)Se2@NiFe LDH hollow nanocages for enhanced oxygen evolution. *ACS Appl. Mater. Interfaces* **2019**, *11*, 8106-8114.
24. Bai, L.; Lee, S.; Hu, X. Spectroscopic and electrokinetic evidence for a bifunctional mechanism of the oxygen evolution reaction. *Angew. Chem. Int. Ed. Engl.* **2021**, *60*, 3095-3103.
25. Gao, Z. W.; Liu, J. Y.; Chen, X. M.; Zheng, X. L.; Mao, J.; Liu, H.; Ma, T.; Li, L.; Wang, W. C.; Du, X. W., Engineering NiO/NiFe LDH intersection to bypass scaling relationship for oxygen evolution reaction via dynamic tridimensional adsorption of intermediates. *Adv Mater* **2019**, *31*, e1804769.
26. Dong, Q.; Wang, Q.; Dai, Z.; Qiu, H.; Dong, X. MOF-derived Zn-doped CoSe2 as an efficient and stable free-standing catalyst for oxygen evolution reaction. *ACS Appl. Mater. Interfaces* **2016**, *8*, 26902-26907.
27. He, K.; Tadesse Tsega, T.; Liu, X.; Zai, J.; Li, X. H.; Liu, X.; Li, W.; Ali, N.; Qian, X. Utilizing the space-charge region of the FeNi-LDH/CuP p-n junction to promote performance in oxygen evolution electrocatalysis. *Angew. Chem., Int. Ed.* **2019**, *58*, 11903-11909.
28. Yang, R.; Zhou, Y.; Xing, Y.; Li, D.; Jiang, D.; Chen, M.; Shi, W.; Yuan, S. Synergistic coupling of CoFe-LDH arrays with NiFe-LDH nanosheet for highly efficient overall water splitting in alkaline media. *Appl. Catal. B Environ.* **2019**, *253*, 131-139.
29. Liu, J.; Wang, J.; Zhang, B.; Ruan, Y.; Lv, L.; Ji, X.; Xu, K.; Miao, L.; Jiang, J. Hierarchical NiCo2S4@NiFe LDH heterostructures supported on nickel foam for enhanced overall-water-splitting activity. *ACS Appl. Mater. Interfaces* **2017**, *9*, 15364-15372.
30. Zhang, F. S.; Wang, J. W.; Luo, J.; Liu, R. R.; Zhang, Z. M.; He, C. T.; Lu, T. B. Extraction of nickel from NiFe-LDH into Ni2P@NiFe hydroxide as a bifunctional electrocatalyst for efficient overall water splitting. *Chem. Sci.* **2018**, *9*, 1375-1384.
31. Jia, B.; Xue, Z.; Liu, Q.; Liu, Q.; Liu, K.; Liu, M.; Chan, T.-S.; Li, Y.; Li, Z.; Su, C.-Y.; Li, G. Hierarchical nanotubes constructed from CoSe2 nanorods with an oxygen-rich surface for an efficient oxygen evolution reaction. *J. Mater. Chem. A* **2019**, *7*, 15073-15078.
32. Kwak, I. H.; Im, H. S.; Jang, D. M.; Kim, Y. W.; Park, K.; Lim, Y. R.; Cha, E. H.; Park, J. CoSe2 and NiSe2 nanocrystals as superior bifunctional catalysts for electrochemical and photoelectrochemical water splitting. *ACS Appl. Mater. Interfaces* **2016**, *8*, 5327-5357.
33. Zhao, S.; Jin, R.; Abroshan, H.; Zeng, C.; Zhang, H.; House, S. D.; Gottlieb, E.; Kim, H. J.; Yang, J. C.; Jin, R., Gold nanoclusters promote electrocatalytic water oxidation at the nanocluster/CoSe2 interface. *J. Am. Chem. Soc.* **2017**, *139*, 1077-1080.